IEEE Access
Multidisciplinary | Rapid Review | Open Access Journal

Received December 5, 2016, accepted January 15, 2017, date of publication February 20, 2017, date of current version March 15, 2017.

Digital Object Identifier 10.1109/ACCESS.2017.2662798

Microfluidic System Protocols for Integrated On-Chip Communications and Cooling

STEFANUS A. WIRDATMADJA[1], DMITRI MOLTCHANOV[1], SASITHARAN BALASUBRAMANIAM[1,2], AND YEVGENI KOUCHERYAVY[1]

[1]Department of Electronics and Communications Engineering, Tampere University of Technology, 33720 Tampere, Finland
[2]Telecommunications Software and Systems Group, Waterford Institute of Technology, IE2 Ireland

Corresponding author: S. A. Wirdatmadja (stefanus.wirdatmadja@tut.fi)

This work was supported in part by the Academy of Finland FiDiPro Program, through the Project Nanocommunication Networks, 2012–2016, in part by the Finnish Academy Research Fellow Program under Project 284531, and in part by the Science Foundation Ireland via the CONNECT Research Centre under Grant 13/RC/2077.

ABSTRACT The advancements in multi-core central processing units have attracted new designs ranging from mechanisms of packing higher number of transistors into the small space, new techniques for communications (e.g., wireless network on chips), or new methodologies for cooling the chip. The latter two design aspects are the focus of this paper, where a microfluidic system is utilized for performing both functions. The miniaturization of microfluidic channels makes it attractive to embed them into the chips to transport fluids that can remove the heat from the processor cores. The extension of the cooling purpose of on-chip microfluidic channels is done by integrating communication feature. The communication process is achieved by transporting fluid through the channel and injecting information through air droplets. Protocols for microfluidic communications are applied, including physical layer functionalities and medium access protocols. The protocol design takes into considerations various properties of the microfludics. Based on the proposed system, the tradeoffs between the data rate and its impact on the amount of heat that can be removed from the processor are evaluated. This system provides new forms of condensed processor design of the future, in which integration of multiple functionalities of microfluidic channel system embedded into multi-core processors.

INDEX TERMS Microfluidics, communications, cooling, protocols.

I. INTRODUCTION

The advancements of communication systems over the years has witnessed increased connectivity between numerous types of devices, large and miniature. The examples of connectivity of miniature scale devices, are the on-chip interconnects [1] and the wireless connections of cores in multi-core processors [2]. While the advanced development of multi-core processors have led to increased number of transistors packed into a small space, and also communication between large number of cores, it has also resulted in increased heat production [3]. In the current processor design, a considerable volume of space is dedicated to removing the thermal heat, while only a small volume is utilized for processing logic [4]. In order to realize beyond **Exa-scale** computers of the future, one proposed approach is 3D architecture, where processors are stacked onto a board to increase computational power. However, with the large volume of space used for removing thermal heat, developing a 3D architecture takes a large amount of space. Inspired by the cooling process of the brain, [4] proposed a liquid cooling solution, where channels of fluids are transported through the processors carrying coolant the remove the heat [5]. The proposed approach, requires fluidic microchannels that run into all processors, where the channels merge at the board and rack level, creating a *"blood vessel"* like fluid network covering the entire data center. Since the fluid networks is transported through the processors, and network between them together, a question remains as to whether other functionalities can also be integrated into the fluid networks - for example, communications. By integrating communications into the fluid networks, vital information from the sensors within the processors, can be transmitted to a central control and monitoring system. This can be achieved by enabling the communication process to piggyback on the fluids, minimizing the need to develop a wired or wireless infrastructure to carry all the sensor information.

The communication process through the fluidic network, could be achieved through *molecular communication* [6]–[8]. The objective of molecular communication is enable communication at the nanoscale, where information can be represented and transported through molecules. Examples of proposed molecular communication systems include diffusion-based communication [9], bacterial nanonetworks [10], as well as FRET [11]. In recent years, a new model of molecular communication has emerged, where information can be transmitted through microfluidic devices [12], which is the focus of this paper. Although the fluidic network goes through the different processors and aggregate together into a larger network and transmits information to the control and monitoring system as illustrated in Fig. 1, in this paper, we only focus on the fluidic communication protocols within a single processors. In particular, we focus on microfluidic communication, where microfluidic channels are laid on the cores of the processors, connecting and providing a communication infrastructure for the sensor, leading to a microfluidic nanoscale on-chip sensor network. The placements of the microfluidic channels on the cores also have the original purpose of removing the heat as the fluid flows through the center of the cores. Due to the physical properties and behaviors of fluids, the communication protocols used in classical communication networks may not directly be adopted and we need to consider a number of properties and challenges found in microfluidic systems. First and foremost, while the fluids pass through the channel as *continuous phase*, the messages inserted into the channels are represented as *dispersed phase*, which could be air or other types of medium such as oil. Secondly, since the flows of fluids that pass through the channels have mass that is far heavier than electrons propagating through a wire, this results in longer propagation time. Thirdly, a different form of interference is found in microfluidic flows where dispersed phase that are too close to each other can lead to coalescence. Therefore, the medium access technique as well as time-slot configurations are highly dependent on accurately detecting incoming dispersed phase, or acquiring knowledge on the channel usage. The medium access depends on the topology of the transmitters and receivers along the channel. Fourthly, the throughput of channel is dependent on equipments used for injecting the dispersed phase, namely the *injector* and the *detector*. Therefore, the accuracy of the throughput is highly dependent on the accuracy of injecting the dispersed phase, as well as detection at the receiver.

In this paper, we propose and evaluate protocols for microfluidic communications. Starting from the physical layer, our contribution includes a feasible modulation techniques that are suitable for microfluidic communications. Then we develop protocols at the data link layer that optimize the transmission medium access for the network entities to avoid coalescence. In this layer we also specify an addressing scheme that supports multiple transmitter and receivers along a bus topology. For each of the protocol layer, we analyze their performance and compare them numerically to viable alternatives. Lastly, as a case study application, we evaluate the microfluidic communication system for a multi-core Central Processing Unit (CPU) sensor networks, by focusing on the impact of data rates and the quantity of heat removed from the processor.

The rest of the paper is organized as follows. In Section II, we introduce the droplet microfluidic systems describing their properties as well as components for the communication systems. Section III discusses the general architecture for the proposed microfluidic communication systems. Section IV presents the physical layer and section V discusses the medium access layer. Section VI presents the case study for the multi-core on-chip integrated communication and cooling, including its performance evaluation. The conclusions are drawn in the last section.

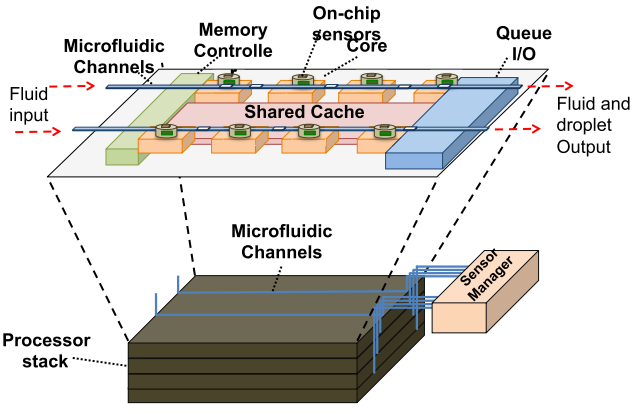

FIGURE 1. Illustration of a multi-core processor on-chip integrated communication and cooling system. Our focus is to utilize the microfluidic channels to provide communications for sensors on the chip.

II. DROPLET MICROFLUIDICS PROPERTIES

A. SYSTEM DESCRIPTION

The structure as well as the components for our proposed microfluidic communication system are shown inx Fig. 2. As illustrated in the figure, the microchannel has a diameter of d and is coupled with a syringe pump that controls the flow for both the dispersed and continuous phases. The air microdroplet generator is a T-junction model, and a laser

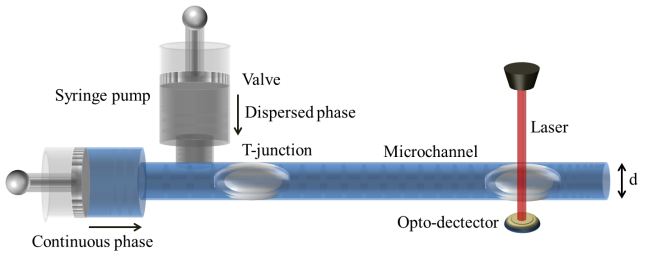

FIGURE 2. Illustration of a droplet-based microfluidic communication system. The components include a micro droplet generator that produces air, which represents the information, as well as an optodetector at the receiver. The syringe pump is used to maintain the continuous flow of water and air that is pushed through the microchannel.

optodetector is used to sense the droplets at the receiver.

A fluid flow in a microfluidic device could fall into any of the following category: (i) *laminar* flow, (ii) *turbulent* flow, or (iii) *transition phase*. An ideal microfluidic channel should maintain the *laminar flow* regime as turbulent effects may negatively affect the air droplet, which in our case represents the transmitted information. The dimensionless parameter describing the flow regime is the *Reynolds number*, (*Re*). A flow is in the laminar state if $Re \leq 2000$. When the liquid with kinematic viscosity ν (m^2/s) flows in a channel with a diameter D_H (m) (assuming cylindrical channel) at a rate of v (m/s), the Reynolds number can be calculated as [13]

$$Re = \frac{vD_H}{\nu}. \tag{1}$$

When dispersed phase is used as information carrier, the flow speed affects the data rate that a microfluidic channel may potentially provide. Fig. 3 demonstrates the Reynolds number as a function of the diameter of the microfluidic channel and flow speed. Observing the presented data, it is noticeable that the smaller diameter of microfluidic channel, the higher is the limit of flow speed to be able to maintain its laminar regime. The area below $Re = 2000$ line indicates that the flow is still laminar. For example, flow speed of 40 m/s is laminar in 50 μm channel, but it is turbulent in the 100 μm channel.

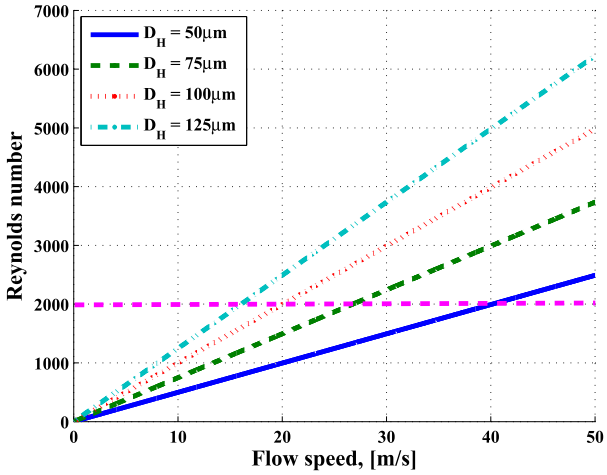

FIGURE 3. **The impact of flow speeds on the Reynolds number for different microchannel diameters.**

The water that we use as a continuous phase is a *Newtonian* fluid which means that the viscosity does not change as the shear or tensile stress is applied. A steady laminar flow of Newtonian fluid depending solely on the applied pressure is characterized as *Poiseuille* flow. Hence, the pressure change along the channel can be calculated as [14]

$$\Delta P = \frac{128\eta L}{\pi D_H^4} Q, \tag{2}$$

where ΔP is a pressure loss (Pa), L (m) is the channel length, η is dynamic viscosity, d (m) is the diameter of the channel, and Q (m^3/s) is the volumetric flow estimated as [14]

$$Q = \lim_{\Delta t \to 0} \frac{\Delta V}{\Delta t} = \frac{dV}{dt} = \iint_A v \cdot dA. \tag{3}$$

When an air microdroplet enters the channel, the pressure change no longer follows (2) and we need to take additional pressure components attributing to the total pressure change. This additional components includes the capillary force pressure and friction force pressure. The capillary pressure is defined as the difference in pressure across the interface between two immiscible fluids. Since there are two interfaces, receding and advancing, it means there are two pressure differences. Therefore, the total pressure ΔP_{total} is represented as [13]

$$\begin{aligned} \Delta P_{total} &= \Delta P_{capillary} + \Delta P_{friction} \\ &= \frac{4\gamma}{d}(\cos\theta_{d,r} - \cos\theta_{d,a}) \\ &\quad + \frac{128Q}{\pi d^4}(\eta_{air} L_{air} + \eta_{water} L_{water}), \end{aligned}$$

where the θ_d is the dynamic contact angle of the droplet and the microchannel, and this is defined as

$$\theta_d = \theta_s + \frac{\kappa \eta v}{3\gamma \theta_s^2}. \tag{4}$$

Furthermore, the pressure difference applied to the microfluidic channel dictates the flow speed of the liquid as [13]

$$v = \sqrt{\frac{\Delta P D_H}{2fL\rho}}. \tag{5}$$

Theoretically, the minimum size of the air droplet equals to the size of the diameter of the microchannel [15]. However, this size of droplet is prone to breakage by flow pressure (even if it is laminar). In order to prevent this, the size, or equivalently the volume of the droplet, has to be reasonably larger. The time slot for one droplet, T_b is closely related to the droplet size which corresponds to the diameter of microchannel, L_b, and the flow speed, v as

$$T_b = \frac{L_b}{v}. \tag{6}$$

Since the L_b parameter is relatively constant following the microchannel hardware specification, parameter T_b can be adjusted by flow speed management. This particular value is crucial in dictating the achievable data rate of the channel, which is discussed later.

In contrast to water which is incompressible, air is categorized as a compressible medium. For the temperature T (K) and absolute pressure P (Pa), most gases of quantity n moles, have a volume V (m^3) which follows this ideal state equation

$$PV = nRT, \tag{7}$$

where R is gas constant $(8.3144621\ J/mol \cdot K)$.

Therefore, when the air microdroplet flows along a channel with pressure changes, the volume of the gas expands/compresses according to the following equation

$$V_2 = V_1 \frac{P_1}{P_2}. \tag{8}$$

This means that in order to maintain a constant droplet size T_b, a stable pressure needs to be applied to the channel. Besides the change in the air droplet size, the minimum distance needs to be taken into account as well since coalescence may happen when the distance between the droplets is small.

III. MICROFLUIDIC COMMUNICATION PROTOCOLS

The overall architecture of the multi-core microfluidic sensor communication and cooling system is illustrated in Fig. 4. Each sensor on the core interfaces to the microfluidic channel and transmits information by encoding information through the microdroplet generator. The droplet that produces air bubbles moves along the flow to the sensor manager, which contains an optodetector.

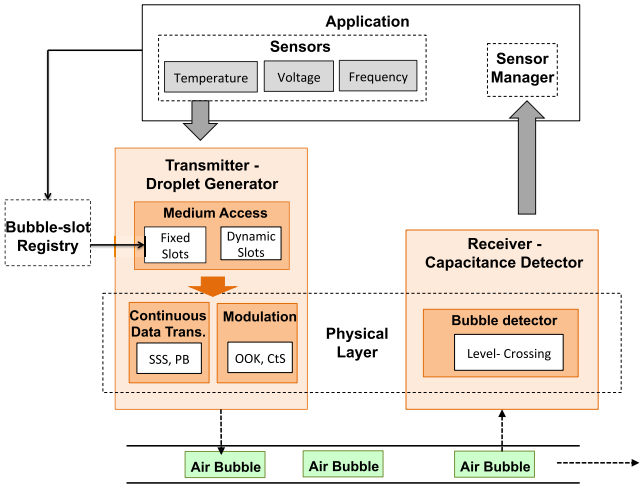

FIGURE 4. The multi-core on-chip sensor network microfluidic communication and cooling architecture.

In this paper we concentrate on two protocol layers for the microfluidic network, which are the physical and the MAC layers. At the physical layer we concentrate on representing data into air droplets that are transmitted through the microchannel. Given the properties of the air droplets, that includes their heavy mass, as well as the varying shapes under pressure and coalescence with other droplets, we propose modulation schemes to compensate and improve the data rates. In order to make guided decisions on these functionalities, we need to assess the noise sources affecting the detection process and then estimate the throughput and *Bit Error Rate* (*BER*) for the physical layer. At the MAC layer we develop access protocols that regulate the production of air droplets, to avoiding coalescence. We address fixed and dynamic time-slots for the access schemes and assess their performance in terms of the number of supported terminals and the rate share they get. Additionally, addressing through dynamic air droplet size is produced by the droplet generator to ensure the sensor manager knows the source.

It is important to emphasize that in this work we do not address upper layer protocols for microfluidic communications. The reason is that these protocols are expected to be very application specific. In our case the application layer is focused on sensors that provide data from the cores. We elaborate further on specifics of this application in Section VI.

IV. PHYSICAL LAYER

In microfluidics communication, the water flow represents the transmission medium. Similarly to electromagnetic communications, the transmitted data can be represented using different modulation scheme. For our on-chip sensor network application, we propose two modulation schemes, which are *On-Off Keying (OOK)* [16] and *Communication through Silence (CtS)* [17].

A. MODULATION SCHEMES

1) OOK AND CTS MODULATIONS

The most common elementary communication form using the presence/absence of symbols to convey bits through a communication channel, is known as *OOK*. In case of the microfluidic channel, the bit "1" can be represented by an air droplet, while the bit "0" – by continuous phase of the fluid. In *OOK*, the time required for a complete message to be transmitted depends on the amount of bits in a message, time slot duration, T_b, and the flow rate, v. In this paper, the "message" and "payload" terms are used interchangeably whose meaning is the dispatched data by the droplet generator in the microfluidic communication system.

The *CtS* is a modulation scheme that relies on the variable delay between the *Start* and the *Stop* bits to convey the information through the communication channel. The process is initiated sending a *Start* bit to a receiver. Each *Start* and *Stop* bits is represented as an air droplet transmitted in a time slot. Upon reception of the bit, a counter is started at the receiver. The assumption is that the operating frequency of both the transmitter and receiver are the same and the clocks are synchronized. As a result, the transmitter knows the counting steps of the receiver. Once the desired value that is to be transmitted is reached, the transmitter transmits a *Stop* bit to the receiver to terminate the counting process. Therefore, the speed of transmission depends on the operating clock frequency, F_c.

Note that the time slot duration of *Start* and *Stop* bits in *CtS* might differ from the time slot duration of a single digit, $T_c = 1/F_c$. Therefore, tuning of F_c is required to maximize the data rate of *CtS* by minimizing the T_c/T_b ratio as illustrated in Fig. 5. However, this is highly dependent on the size of T_b, which depends on the capability of the droplet generator in producing the droplet at the smallest size.

In the microfluidic communication system, the end-to-end delay includes the minimum delay, $T_{\min}$, between the *Start* and *Stop* bits and the payload itself. The minimum delay

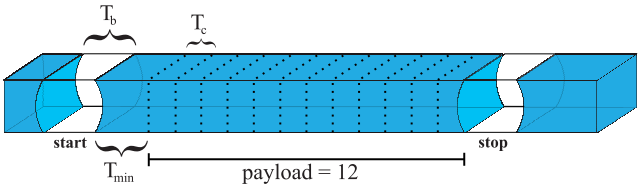

FIGURE 5. CtS modulation scheme transmitting decimal-based payload.

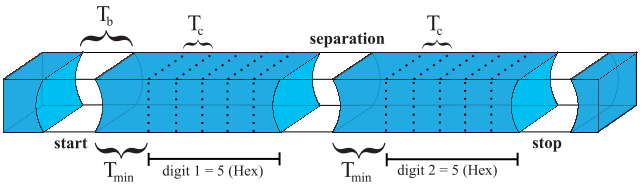

FIGURE 6. Hexadecimal CtS transmitting ASCII character "U" (code="55"). As shown in the figure, two separate transmissions are performed for each symbol.

could be set to a single duration of a symbol, T_c. In what follows, we assume that the payload size is an integer multiple of the operating clock frequency of the system, F_c and the minimum delay, representing the value 0, is set to exactly one clock period. From these requirements it is easy to see that clocks at the sending and receiving sides must be synchronized to avoid the wrong interpretation of the message in *CtS*.

Another property of *CtS* that can be manipulated to increase the data rate, is the base number of bits. For example, the authors in [18] demonstrated that by transforming the values from decimal to hexadecimal base, one could increase the data rate of the scheme. The choice of the number-base format not only dictates the duration of symbols but may require additional control sequences, e.g., separators between digits. For example, for hexadecimal format we need three droplets resulting in three minimum gaps, $T_{\min}$. However, for decimal format we need only two droplets resulting in two minimum gaps $T_{\min}$. Fig. 6 illustrates transmission of hexadecimal letter "*U*".

2) CONTINUOUS DATA TRANSMISSION PROTOCOL

The procedure of continuous data transmission can affect the achievable data rate of *CtS*. We propose two approaches to enable continuous transmission of data. The first is to use *Single Start/Stop* (*SSS*) method, where each payload has its own pair of *Start* and *Stop* indicators as illustrated in Fig. 7(a). Alternatively, one could use more efficient *Piggyback* (*PB*) method, where two consecutive payloads have one common *Start* and *Stop* symbol as illustrated in Fig. 7(b). To enable this scheme consecutive payloads must be first rearranged in the increasing order prior to transmission. Thus, the data rate provided by *PB* approach depends on the availability of data at the transmitter.

To minimize the probability of wrong interpretation of a symbol in *CtS*, a suitable air droplet detection method is required. The implementation of the detector should be precise to avoid mismatch in the counting process, which can lead to interpretation of different values. Exploiting the light propagation properties of fluids for detection purpose can be done by using an optodetector. The optodetector measures the light attenuation between air and water. The large difference in value indicates that detected value is distinguishable enough by using level-crossing detection method. Fig. 8 shows the illustration of the optodetector's output and detection region definition on the corresponding threshold level. As one may observe the change in the voltage level is drastic even for such a small microfluidic channel allowing for accurate detection of air droplets.

B. PERFORMANCE ANALYSIS

1) DATA RATES

In the case of *OOK*, the maximum data rate is fully determined by the physical constraints of the system, particularly, the minimum achievable air droplet size for a given diameter of a channel. On the other hand, *CtS* allows the rate to be controlled externally by manipulating the clock frequency of transceivers. Recall that for both modulation schemes, the value of the droplet duration, T_b, is related to flow velocity, v, and width of the droplet, L_b, as $T_b = L_b/v$.

For *OOK*, both logical "*1*" and "*0*" have the same time slot duration T_b. Therefore, the data rate in bits per second (bps) can be computed as [19]

$$R_{OOK} = \frac{1}{T_b} = \frac{v}{L_b}. \tag{9}$$

For *CtS*, the data rate depends on the number-base of the data (e.g., decimal, hexadecimal) and the continuous data transmission protocol used (*SSS* or *PB*). When decimal base is employed, the total delay D_{DEC} corresponding to n-bits payload between the *Start* and *Stop* symbols is

$$D_{DEC} = T_{min} + \frac{2^n - 1}{F_c} = T_{min} + \frac{P_{DEC}}{F_c}, \quad n \in \mathbb{Z}^*, \tag{10}$$

where P_{DEC} is decimal-based data representation and $T_{\min}$ is the time period which corresponds to the minimum gap/distance between the air droplets to avoid coalescence.

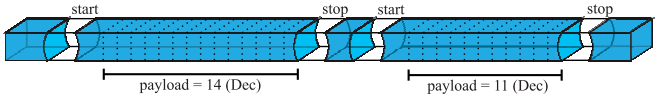

(a) Decimal CtS with single start/stop.

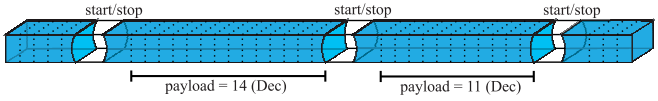

(b) Decimal CtS with piggyback.

FIGURE 7. Communication through silence (CtS) modulation scheme. (a) Decimal CtS with single start/stop. (b) Decimal CtS with piggyback.

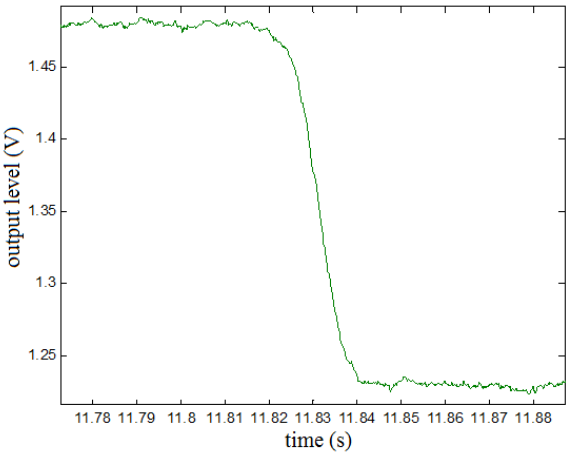

FIGURE 8. Illustration of level change at the optodetector's output when passing the border between two different substances of water and air.

Thus, for the *SSS* continuous data transmission protocol the data rate

$$R_{DEC,SSS} = \frac{n}{2T_b + 2T_{min} + \dfrac{2^n - 1}{F_c}} = \frac{n}{2T_b + T_{min} + D_{DEC}}. \tag{11}$$

while for the *PB* method the data rate is

$$R_{DEC,PB} = \frac{n}{T_b + T_{min} + \dfrac{2^n - 1}{F_c}} = \frac{n}{T_b + D_{DEC}}, \tag{12}$$

Another base representation that we consider is hexadecimal. The total delay D_{HEX} for n-bits payload between *Start* and *Stop* symbols is

$$\begin{aligned} D_{HEX} &= T_b + 2T_{min} + \frac{P_{DEC} - \left(15 \times \left\lfloor \dfrac{P_{DEC}}{16} \right\rfloor\right)}{F_c} \\ &= T_b + 2T_{min} + \frac{P_{HEX}}{F_c}, \quad n = 0, 1, \ldots, 8. \end{aligned}$$

where P_{HEX} is the hexadecimal-based data representation.

For the continuous data transmission protocol *SSS*, the data rate $DR_{HEX,SSS}$ is represented as

$$R_{HEX,SSS} = \frac{n}{3T_b + 3T_{\min} + \dfrac{P_{HEX}}{F_c}} = \frac{n}{2T_b + T_{\min} + D_{HEX}}. \tag{13}$$

while for the *PB* method the data rate is represented as

$$R_{HEX,PB} = \frac{n}{2T_b + 2T_{\min} + \dfrac{P_{HEX}}{F_c}} = \frac{n}{T_b + D_{HEX}} \tag{14}$$

The performance of both *OOK* and *CtS* modulations is shown in Fig. 9, and the parameters are presented in Table 1. For the *CtS* scheme, we consider both continuous data transmission protocols *SSS* and *PB* for the two encoding schemes.

TABLE 1. Simulation Parameters

Parameter	Value [Unit]	Description
Channel Diameter	50||100 [μm]	Hydraulic Diameter
T_b for $L_b = 50\mu m$	6.52 [ms]	Time slot for $L_b = 50\mu m$
T_b for $L_b = 100\mu m$	13 [ms]	Time slot for $L_b = 100\mu m$
v	7.667 [mm/s]	Flow speed
Modulation scheme	*OOK, CtS*	Decimal, Hexadecimal
Transmission scheme	*PB, SSS*	Piggyback, Sgl Start/Stop
Transmitted bits	8 [$bits$]	Binary

The data rate as a function of the air droplet duration is shown in Fig. 9(a). As one may expect, the performance of all modulations drops when the air droplet size becomes larger. It is important to note that the performance of *OOK* for the minimum droplet size $L_b = 50\mu m$ (recall that it coincides with the diameter of a microfluidic channel) is second best compared to all *CtS* schemes considered. In fact, only hexadecimal *CtS* with operating frequency $F_c = 3$MHz outperforms this. The reason for this behavior is that in *CtS* we still need to use two droplets for the *Start* and *Stop* symbols. For larger payload sizes, better performance gains are expected for *CtS*. Also, the increase in L_b affects the total transmission length and time for *OOK* more compared to *CtS*, and this is because the payload of *CtS* is dictated by the operating frequency and not by L_b.

Fig. 9(b) demonstrates the achieved data rates as a function of the operating frequency, F_c, for both *OOK* and *CtS* and the droplet sizes $50\mu m$ and $100\mu m$. Since the operational frequency has no correlation with the *OOK* scheme, the data rate of *OOK* is constant. However, for $L_b = 50\mu m$ the performance of *OOK* is better than for all *CtS* schemes except the hexadecimal CtS across majority of the frequency domain. Here, one may also notice that the decimal *CtS* performs significantly worse than the hexadecimal because 8 binary bits in decimal causes longer delay than in hexadecimal. Finally, the achieved data rate for *CtS* and *OOK* as a function of the payload size (in terms of binary bits) is shown in Fig. 9(c) for the droplet sizes $50\mu m$ and $100\mu m$, and operating frequency $F_c = 3$MHz. This figure is quite illustrative as it shows that for the *CtS* scheme there is an optimal message size that results in the best data rate. This optimal size is a function of the minimum air droplet L_b. In the case of *OOK*, the data rate is independent of the air droplet size.

Performance of *OOK* and *CtS* modulations operating in the continuous data transmission protocol *SSS* regime is demonstrated in Fig. 10. Qualitatively the behavior of all dependencies is similar to that of *CtS* with continuous transmission protocol *PB*. However, it is important to note that quantitatively *OOK* performs even better compared to *CtS* operating in continuous data transmission protocol *SSS* regime. Only hexadecimal *CtS* operating at 3MHz performs better than *OOK*. This occurs due to the characteristic of *SSS* itself where indicator bits (start/separation/stop) occupy relatively large space compared to the payload data.

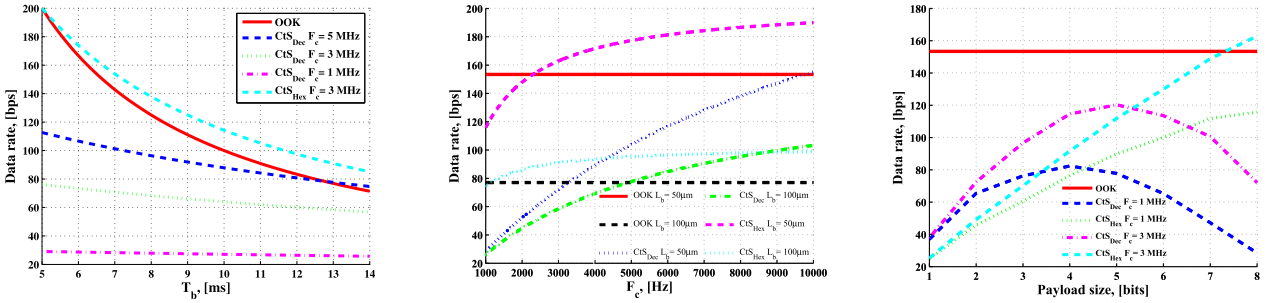

(a) Data rate as a function of T_b. (b) Data rate as a function of F_c. (c) Data rate as a function of payload.

FIGURE 9. Performance comparison of *OOK* and *CtS* modulation schemes using the *PB* continuous data protocol. (a) Data rate as a function of T_b. (b) Data rate as a function of F_c. (c) Data rate as a function of payload.

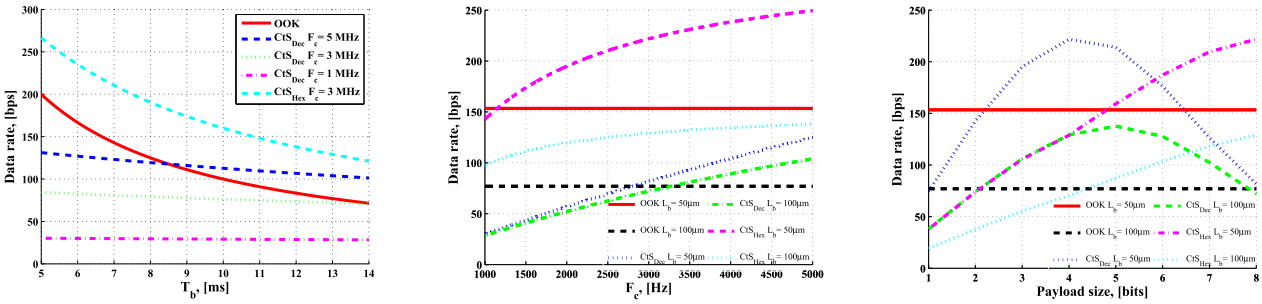

(a) Data rate as a function of T_b. (b) Data rate as a function of F_c. (c) Data rate as a function of payload.

FIGURE 10. Performance comparison of *OOK* and *CtS* modulation scheme using the *SSS* continuous data protocol. (a) Data rate as a function of T_b. (b) Data rate as a function of F_c. (c) Data rate as a function of payload.

C. SYMBOL ERROR RATE (SER) AND THROUGHPUT

The raw data rate provided by a modulation schemes does not completely characterize their channel performance as we need to ensure that the *BER* is kept at the acceptable level. The latter requires us to address factors affecting the reception of air droplets at the receiving side. These factors contribute to the noise in the microfluidic channel. There are three types of noises affecting the reception of symbols:

Injection-inaccuracy noise. The microdroplet generator may be inaccurate in terms of injection time and injected microdroplet volume/size. This noise factor is related to inaccuracy of injection equipment that can be sufficiently well modeled using the zero-mean Gaussian distribution with a certain variance σ_I^2 [20].

Pressure-maintenance noise. Pressure instability is related to velocity fluctuations along the transmission channel. Similarly to injection-inaccuracy noise, this components is related to imperfections of one of the subsystems and can be modeled using zero-mean Gaussian distribution with variance σ_P^2 [20].

Detection noise. The detector output is also affected by non-ideal operation of the droplet detection apparatus. A number of studies suggested that this noise could be represented using zero-mean Gaussian distribution with variance σ_D^2. Fig. 11 shows the empirical distribution of the optodetector noise in presence of continuous phase in the channel we obtained in our experiments and its approximation by Normal distribution.

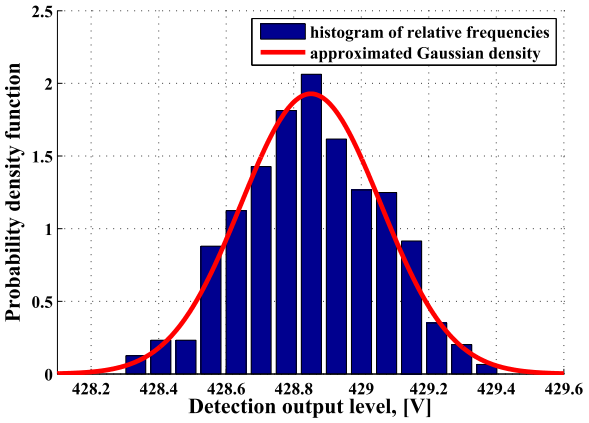

FIGURE 11. Detection noise density based on optodector receivers. The noise measures the deviations of the air droplet size observed at the receiver.

Let us denote the injection-inaccuracy, pressure maintenance and detection noises by random variables $\mathcal{N}_I(0, \sigma_I^2)$, $\mathcal{N}_P(0, \sigma_P^2)$, and $\mathcal{N}_D(0, \sigma_D^2)$, respectively. Since these noises are produced by different elements of the system that do not interfere with each other they are additive in nature and may add up either constructively or destructively at the receiver. Further observe that injection-inaccuracy noise is source-

induced noise implying that its effect at the receiver depends on the distance between communicating systems l. We take this into account by properly scaling the random variable by a coefficient $k_I(l)$. The second term is independent of the location of transceivers while the last term depends on the local phenomenon at the receiving side. Thus, the overall loss process follows zero-mean Gaussian random variable with variance

$$\sigma_E^2(l) = k_I^2(l)\sigma_I^2 + \sigma_P^2 + \sigma_D^2. \tag{15}$$

For *OOK* modulation, the error in detection happens when bit "*1*" is detected as "*0*" and vice versa. This happens when the threshold time slot for that particular bit is not fulfilled (too long or too short) causing false interpretation of the bit. The minimum time duration of one time slot for bit "*1*" which corresponds to the minimum droplet length is T_b and the minimum time duration of one time slot for bit "0" which corresponds to the minimum distance between droplets is T_{min}, where $T_b = T_{min} = D_H$ (D_H is the hydraulic diameter). The calculation of *SER* for *OOK* and *CtS* modulations is conceptually similar and provided next for the case of *CtS*.

In a *CtS* transmission system whose operating frequency is F_c, the tolerable time bias equals to half of the one signal period, $\frac{T_c}{2}$. The detected symbol is received correctly if its value lies between $\pm\frac{T_c}{2}$. On the other hand, if it falls outside a given range, the symbol is considered as erroneously received. Fig. 12 shows the probability density function for Gaussian noise. Here, the received symbol $\hat{x}$ is correctly detected when it lies in the green-shaded region while the gray-shaded region indicates incorrect detection. Recall that the detected data are the original data with the accumulative system noise, $\mathcal{N}_{err}(0, \sigma_{err}^2)$.

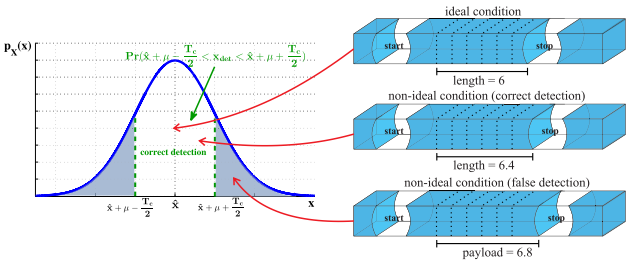

FIGURE 12. Illustration of the symbol detection process.

Using Q-function the *SER* is

$$p_E(l) = 2Pr\left(x > \hat{x} + \mu + \frac{T_c}{2}\right) = 2\left(\int_{\hat{x}+\mu+\frac{T_c}{2}}^{\infty} p_X(x)\,\mathrm{d}x\right)$$
$$= 2Q\left(\frac{\left(\hat{x} + \mu + \frac{T_c}{2}\right) - \hat{x}}{\sigma_E(l)}\right) = 2Q\left(\frac{T_c}{2\sigma_E(l)}\right),$$

where $\hat{x}$ is transmitted symbol.

Excluding false detection from the data rate calculation, the throughput of the system is defined as the fraction of symbols that are received correctly. Therefore, based on the data rate for different modulation schemes, R, and the *SER* p_E, the throughput T_H is represented as

$$T_H = R[1 - p_E(l)]. \tag{16}$$

V. MEDIUM ACCESS CONTROL LAYER

In this section, we discuss the medium access control protocols with respect to the properties of the air droplets used for the transmission.

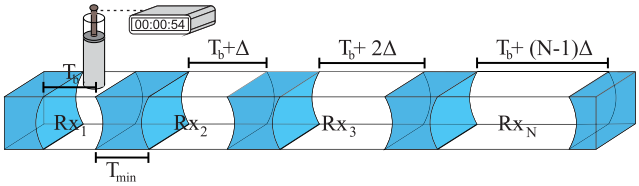

FIGURE 13. Physical addressing in microfluidic communications.

A. ADDRESSING

Addressing is an essential feature of the MAC layers allowing for communications between different pair of stations. We propose the use of *Physical Addressing* which uses the properties of microfluidics. Fig. 13 illustrates our proposed addressing scheme that is applicable for multiple transmitter/receiver design of microfluidic communication systems. The addressing is provided by the length of the droplet itself. In *CtS* communications these droplets represent the *Start* and *Stop* bits while in *OOK* they are used to represent the duration of 0 and 1 symbols. Since T_b is the minimum time-slot allowed for the air droplet, the length of the time-slot corresponding to each particular source/destination pair is obtained by adding a certain fraction of T_b, Δ_{T_b}. Assuming N receivers and denoting the time slot length for the receiver i by $T_{b,i}$ we have

$$T_{b,i} = T_b + [(i-1)\Delta_{T_b}], \quad i = 1, 2, \ldots, N. \tag{17}$$

Application of the proposed scheme results in different sizes of air droplets, which provides the capability to distinguish between different transmitters by simply measuring the duration of the droplet at the receiver. Note that the value of Δ_{T_b} should be small enough to minimize the amount of control information, but sufficiently large for reliable detection of differences between droplet sizes. Consequently, as the number of transmitters increase, the amount of control information grows proportionally to the value of Δ_{T_b} implying that the physical addressing is suitable for a small, possibly local network.

B. FIXED AND DYNAMIC TIME-SLOTS ACCESS

In principle, microfluidic communication systems can rely on similar principles for channel access as electromagnetic networks. However, unlike conventional electrical signaling in computer networks, the microfluidic channel requires unidirectional ordered transmission of air droplets between the

transmitters and receivers. Therefore, the design architecture of the system must take into account the order of the droplet transmitter positions, and possibly arranging stations in a certain order and using the *Time Division Multiple Access* (*TDMA*) for droplet injection into the fluid medium. Both *fixed* and *dynamic time-slot access* are discussed by considering the approach that maximizes the channel utilization and collision avoidance.

1) DYNAMIC TIME-SLOT ACCESS SCHEME

In Dynamic Time-Slot access scheme, the medium is divided into time slots of the length sufficient to send the minimum payload size. There is a *Droplet Registry Unit* (*DRU*) serving as a coordination entity having the full knowledge of the system including traffic demands on the stations and scheduling transmission of end systems by exclusively allocating the exact required number of time slots for each transmitter. All the transmitters are equipped with special wired interfaces to the *DRU*. The amount of information exchanged between end systems and the *DRU* may vary depending on a particular scheduling algorithm used. Fig. 14 shows how the droplet transmitters are connected to a *DRU* which manages the transmission channel access scheduling. The *DRU* is responsible for time-length-volume conversion, synchronization, and air droplets position tracking.

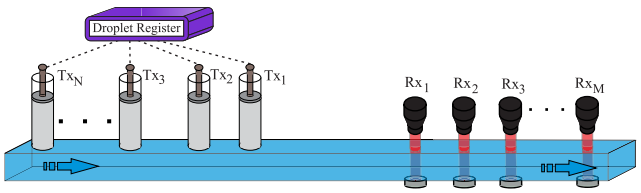

FIGURE 14. An illustration of the dynamic time-slot access scheme, where the *DRU* controls the microdroplet generator for deceasing the air droplets.

Depending on the amount of information exchanged via wired interfaces we envision two feasible scheduling schemes for the dynamic time-slot access:

Payload-based (PB) Scheduling. In this scheme, the *DRU* requires the information about the payload size that are at the *Head of Lines* (*HOL*) of the droplet transmitting stations. Even though this scheme burdens the *DRU*, it maximizes the utilization of the microfluidic channel. In particular, when the application tries to transmit decimal payload L_d, the *DRU* calculates the vacant space in the microfluidic channel $L_{T,i}$ as

$$L_{T,i} = 2[L_b + L_{\min} + \Delta(i-1)] + L_d, \qquad (18)$$

where L_b denotes the minimum droplet length (we convert T_b to L_b), Δ is the length between the droplet transmitters, i is the order of droplet transmitter which corresponds to its address, and $L_{\min}$ is the minimum distance between air droplets to avoid coalescence (we converted $T_{\min}$ to $L_{\min}$).

Maximum-Time-Based (MTB) Scheduling. In this scheme, the *DRU* does not need the knowledge of the *HOL* payload. The time allocation is based on the maximum required slot for the particular microdroplet generator. The *DRU* has to ensure the vacant space which is represented as follows,

$$L_{T,i} = 2[L_b + L_{\min} + \Delta(i-1)] + L_{d\_max}, \qquad (19)$$

where L_{d_max} is the threshold of payload length.

2) FIXED TIME-SLOT ACCESS SCHEME

When there is no control entity such as the *DRU*, a different approach should be used. In this case, the process of accessing the microfluidic channel to inject droplets is similar to injecting packets into the bus, where combined schemes of *TDMA* and *Collision Sense Multiple Access* (*CSMA*) protocols can be used. However, the conventional *CSMA* sensing process needs to be modified for use in microfluidic communication system.

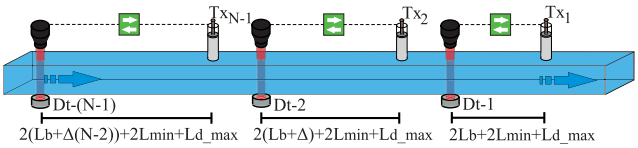

FIGURE 15. An illustration of the architecture for the fixed time-slot access scheme, where each droplet transmitter is equipped with a capacitor detector that serves as carrier sensing for the channel.

Fig. 15 illustrates the architecture for the fixed time-slot access scheme for microfluidic communication system that incorporates CSMA sensing. As shown in the figure, each droplet transmitter has an optodector, which serves as the carrier sensor. The maximum transmitted message might be different from one microdroplet generator to another and it depends on the defined payload format. Thus, the detector distance from the corresponding microdroplet generator follows (19).

If the fairness of resource allocation is of interest, an additional algorithm is required. Indeed, if no additional efforts is taken, a transmitter located at position i does not take into considerations the transmission opportunities of stations located at positions $i+1, i+2, \ldots, N$. Therefore, a transmitter with high traffic demands located in the beginning of the microfluidic system may occupy the channel for majority of the time. In order to counter this issue, priority based access can be utilized where the priority relation between the microdroplet generator for the system should be chosen such that

$$P^{(1)} < P^{(2)} < P^{(3)} < \cdots < P^{(N-1)} < P^{(N)}, \qquad (20)$$

where $P^{(i)}$ is the priority of the microdroplet generator i.

Fig. 16 shows the structure of time slots for the air droplet which includes slots for each droplet transmitters in the system. The T_{min} slot ensures minimum distance needed to avoid coalescence with the next droplet. For slots which

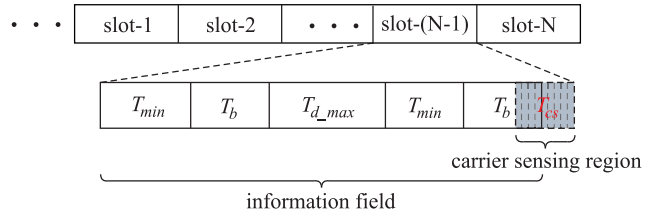

FIGURE 16. Structure of Time Slots of TDMA Scheduling.

bring information from the transmitters, each of them consists of uniform carrier sensing region which overlaps with the address indicator droplet. This carrier sensing region is divided into several smaller fields for each particular microdroplet generator to start its addressing transmission.

For one full cycle of N microdroplet transmitters consisting of N time slots, the duration of a slot is

$$T_{slot} = 2(T_{b,N} + T_{\min}) + T_{d\_max} + T_{cs}. \quad (21)$$

where $T_{b,N}$ is the time duration of maximum data to be transmitted in the N^{th} slot which is the microdroplet generator whose address is the longest among all other transmitters, and T_{cs} is time duration for carrier sensing.

In order to maximize the occupancy of the channel, a transmitter senses all the the time slots which, by default, belong to the preceding transmitters. If some of them are vacant, they can be used for data transmission. Observe that such behavior naturally leads to unfairness of the slots allocation along the microfluidic channel as microdroplet generators located in the middle of the order have more resources than those at the end or at the beginning. To address this issue the following probabilistic access scheme is proposed. Let γ_i be the probability of occupying a preceding time slots by microdroplet generator i. Assuming that the air droplet generation probabilities of all the stations, $p_j, j = 1, 2, \ldots, N$, are known the optimal values of γ_i providing fairness of resource allocation are given by

$$\gamma_i = \frac{p_i}{\sum_{j=i}^{N} p_j}, \quad i = 2, 3, \ldots, N \quad (22)$$

which is valid for arbitrary values of p_i.

Assuming constant $p_i = p, i = 1, 2 \ldots, N$ we have

$$\gamma_i = \frac{p}{\sum_{j=i}^{N} p} = \frac{1}{(N - i + 1)}, \quad i = 2, 3, \ldots, N. \quad (23)$$

C. PERFORMANCE ANALYSIS

In the dynamic time-slot access scheme, where the *DRU* manages the access to the transmission medium, the throughput calculation is simple. Based on the knowledge of a certain scheduling process at the *DRU* (e.g., fair or weighted fair queuing) and equal traffic requirements for all the microdroplet generator, we can directly obtain the throughput for the whole system.

Fig. 17 demonstrates per-microdroplet generator throughput for two and three generator design with fixed time-slot

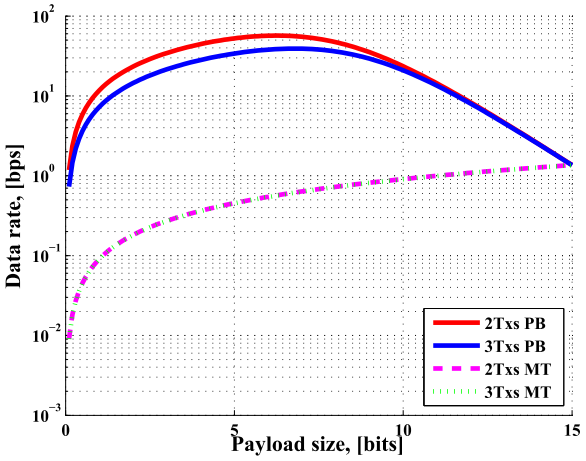

FIGURE 17. Aggregate throughput as a function of F_c for varying number of microdroplet generator.

access of *PB* and *MTB* scheduling for $F_c = 3$MHz. For the *PB* scheduling, the *DRU* has full knowledge of the payload size while in case of *MTB*, the maximum time slot size is used and is common for all the microdroplet generators. The guard slots between messages are all $L_{min} = 50\mu m$. All the microdroplet generators are assumed to have equal amount of traffic to send in each cycle.

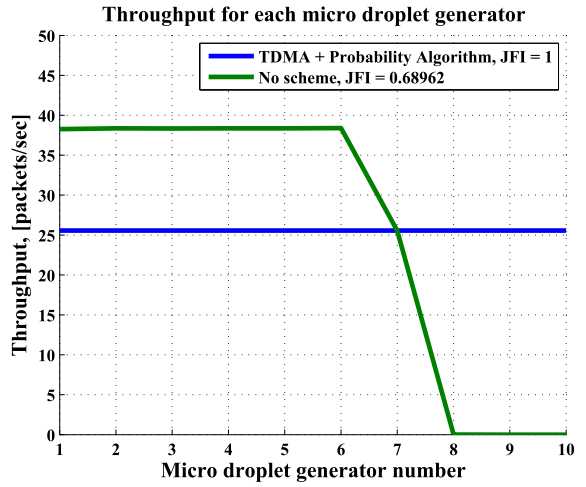

FIGURE 18. The *Jain fairness index* evaluation for per-microdroplet generator throughput.

For fixed time-slot access scheme system ensuring fairness among the microdroplet generators is more complex. Below we evaluate the performance of the proposed algorithm using the simulation approach. In this simulation (Fig. 18), ten microdroplet generators are used to analyze the fairness of the system for one million transmission cycles, and for this we use the *Jain fairness index*. The *Jain fairness index* indicates the fairness measurement of the system and is calculated as:

$$\mathcal{J}(x_1, x_2, \ldots, x_n) = \frac{(\sum_{i=1}^{n} x_i)^2}{n \cdot \sum_{i=1}^{n} x_i^2} \quad (24)$$

where n is the total amount of microdroplet generators, and x_i is the throughput for the i^{th} generator. For this fairness of a fixed time-slot access scheme system simulation, the data generation for all microdroplet generators is equal. The speed of data generation level is average. This means that there is a certain period when the microdroplet generators have a data queue on their buffers. On the other hand, there is also a certain period when the microdroplet generators have sufficient resources to dispatch all the queued data and clear their buffers. From this simulation, the Jain fairness index can be evaluated for this transmission algorithm. The index is equal to "1" which means the system is fair from the throughput and resource allocation point of view.

VI. INTEGRATED MULTI-CORE CPU COMMUNICATIONS AND COOLING

The development of CPU technology has been significant increased in the number of transistors that are packed into small volume of space in order to provide unprecedented level of performance of parallelism. While the increased performance has provided numerous new opportunities with computing power, a major concern is the increased heating in CPUs. Besides efficiency of maintaining stable temperature to minimize damage to the circuitry, sufficient energy is also required to maintain cooling for the CPUs. Air cooling systems are a common solution due to their simplicity and low cost. Similarly, macro liquid cooling systems are also used due to their effectiveness and reliability. However, this technology is only limited to high-end CPUs and GPUs. Furthermore, both air and macro liquid cooling systems requires large space. Another issue with air cooling is the noise affects, and at the same time high power consumption. It has been shown that microchannel liquid cooling system for 3D chip architecture [21] can reduce the overall size of the CPU and maintain good thermal level [21]–[23], [24]. In most of these solutions, a layered design is proposed, where microchannels are embedded deep into the CPU with flowing liquid coolant to absorb the heat radiated from the electrical circuits.

A. PROPOSED ON-CHIP COOLING AND COMMUNICATION ARCHITECTURE

The design of the proposed system is illustrated in Fig. 19. As a reference, we consider the structure of modern multi-core CPU based on a recently released *Intel Core i7-5960X*

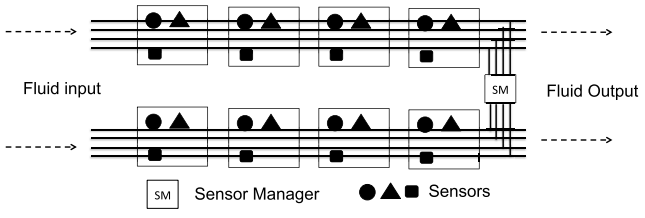

FIGURE 19. The eight-core processor with integrated microfluidic communication and cooling system. The communication channels transport the data from the sensors to the *Sensor Manager*.

TABLE 2. Cooling System Simulation Parameters

Parameter	Value [Unit]
TDP (Intel Core i3)	35 $[W]$
TDP (Intel Core i5)	65 $[W]$
TDP (Intel Core i7)	88 $[W]$
Processor Dimension	$37.5 \times 37.5[mm^2]$
T_{water}	20 $[^oC]$
Channel Width	50 $[\mu m]$
Channel Length	4 $[cm]$
c_p (Water)	4185.5 $[J/kgK]$
c_p (Air)	1005 $[J/kgK]$
ρ (Water)	998.2071 $[kg/m^3K]$
ρ (Air)	1.205 $[kg/m^3K]$

processor, the first 8-core desktop processor with 22nm fabrication process using the *Haswell-E* architecture with the die size of $17.6mm \times 20.2mm$. Eight cores are distributed on the sides with shared 20MB L3 cache in the middle. The CPU runs at 3 GHz base clock and 3.5 GHz turbo regime. The clock is kept on that level in order to maintain the *Thermal Design Power* (*TDP*) at 140W when supporting 8 cores. To monitor the temperature, *Digital Temperature Sensor* (*DTS*) is embedded to each core. The temperature related data includes the difference between the instantaneous temperature and maximum junction temperature. The *DTS* is located near the hottest part of the core and the data from all the *DTSs* is transported over the microfluidic sensor network, including other sensor data as well. By transporting the temperature data to the *Sensor Manager* on the processor, can lead to an adaptive cooling system.

B. COOLING AND DATA-RATE TRADE-OFFS

There are a number of trade-offs in the proposed system. First of all, observe that the *DTS* can be configured to send data periodically causing flow rate adjustment at certain time intervals. Alternatively, they can be configured to report data to the *Sensor Manager* in the events of overheating. Either way, the overall data rate affects the amount of heat absorbed by the coolant as more data implies more air in the channel which leads to lower heat absorption. Secondly, the higher coolant flow rate also leads to higher heat absorption rate. In this section, we evaluate the performance of our proposed system by considering these issues. The parameters used in our performance evaluation are presented in Table 2. Both water and air cooling are based on the same principle of convective heat transfer and thus can be analyzed using the same approach. Assuming that the amount of required cooling is only on the contact surface of the core, we can calculate the heat energy dissipated on the area as [25]

$$q^* = \frac{E_{TDP}}{A_{CPU}}(L_{ch}W_{ch}) \tag{25}$$

where E_{TDP} is the peak heat energy that the core might generate, A_{CPU} is the surface area of a core, and L_{ch} and W_{ch} are the contact length and width of the microfluidic channel with the core surface. Based on this we can obtain the mass

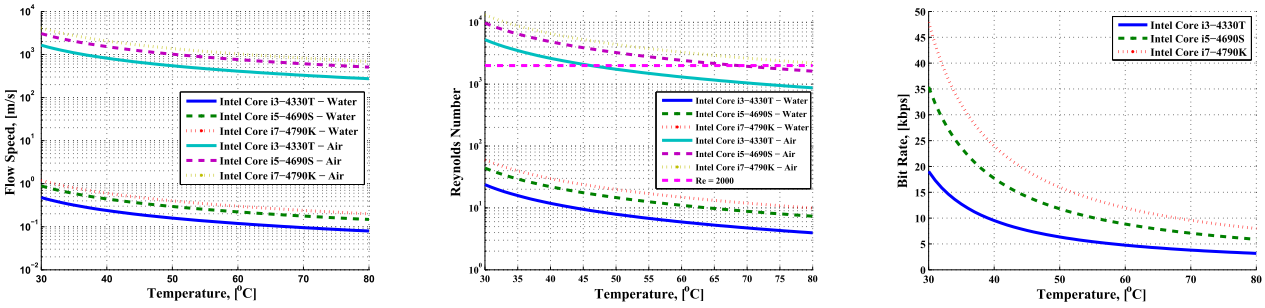

(a) (b) (c)

FIGURE 20. Cooling system analysis. (a) Speed of coolants, 50μm. (b) Reynolds number, 50μm. (c) Bit rates vs. equilibrium temperature.

flow rate of the coolant, whose specific heat capacity C_p is needed to absorb the dissipated heat energy with initial coolant temperature T_1 and equilibrium temperature T_2 as

$$m^* = \frac{q^*}{C_p(T_2 - T_1)} = \frac{q^*}{C_p \Delta T} \tag{26}$$

Finally, we can estimate the average speed of the coolant, v, whose density is ρ in the microchannel with a cross section area of A_{ch}, as

$$v = \frac{m^*}{\rho A_{ch}} \tag{27}$$

In addition, to ensure that the required flow speed is still laminar, we need to calculate the Reynolds number as

$$Re = \frac{vD_H}{\nu} \tag{28}$$

where ν is kinematic viscosity of the coolant.

The results of the analysis are presented in Fig. 20. The required flow speed of continuous phase of water and microdroplets to achieve corresponding equilibrium temperature for three Intel Core family processors is illustrated in Fig. 20(a). This figure is of interest, as it shows the proportional relationship between the cooling process and the flow speed of the continuous phase. As the coolant flows faster, the absorbed amount of heat becomes larger causing lower processor temperature. Fig. 20(b) shows the *Reynolds* number for the microdroplets and continuous phase coolants as a function of equilibrium temperature. We compare our system with air flow based system. It can be seen that to obtain a certain equilibrium temperature, the flow of the air is in turbulent region, while the flow of the water is still in the laminar region. The purple-dashed line indicates the border between the laminar and the turbulent regions. Finally, Fig. 20(c) illustrates the data rates as a function of equilibrium temperature for the three different Intel CPUs. It is important to note that the data rate is directly related to the flow rate. Consequently, higher data rate results in lower equilibrium temperature of the processor.

VII. CONCLUSIONS

The advancements in multi-core processor technology continues to produce devices with high computational capabilities. However, this has also led to increased heat dissipation, calling for new efficient cooling solutions. One viable solution is through integrating microchannels into the processors, where these channels transport fluids to maintain the equilibrium temperature of the chip. In this paper, we propose integrating another functionality into the microchannels used for cooling, and that is communication. The paper starts by defining new modulation schemes at the physical layer, where *On-Off Keying* and *Communication through Silence* is proposed. This is coupled with continuous data transmission protocols that include *Piggy-back* as well as *Single Start/Stop* schemes. On top of the physical layer, medium access control protocols have also been introduced, where schemes found in conventional communication networks have been adopted to suit the properties of microfluidic systems. This includes fixed and dynamic time-slot access schemes. An addressing process is also proposed by controlling the length of air droplets that are injected into the channel. Lastly, a case study on integrated multi-core communication and cooling system is evaluated, based on an on-chip sensor network application, to determine the impact of data transmissions on the temperature of the processor. We believe that the integration of multiple functionalities such as communication and cooling into the on-chip microfluidic system could open new opportunities for processor design of the future, in particular, as we move towards 3D architectures.

REFERENCES

[1] S. Kumar and R. Sharma, "Analytical model for resistivity and mean free path in on-chip interconnects with rough surfaces," *IEEE Trans. Emerg. Topics Comput.*, 2016.

[2] S. Abadal, M. Iannazzo, M. Nemirovsky, A. Cabellos-Aparicio, H. Lee, and E. Alarcón, "On the area and energy scalability of wireless network-on-chip: A model-based benchmarked design space exploration," *IEEE/ACM Trans. Netw.*, vol. 23, no. 5, pp. 1501–1513, Oct. 2015.

[3] A. Bartolini, M. Cacciari, A. Tilli, and L. Benini, "Thermal and energy management of high-performance multicores: Distributed and self-calibrating model-predictive controller," *IEEE Trans. Parallel Distrib. Syst.*, vol. 24, no. 1, pp. 170–183, Jan. 2013.

[4] P. Ruch, T. Brunschwiler, S. Paredes, I. Meijer, and B. Michel, "Roadmap towards ultimately-efficient zeta-scale datacenters," in *Proc. Conf. Design, Autom. Test Eur.*, 2013, pp. 1339–1344.
[5] M. M. Sabry, A. Sridhar, D. Atienza, P. Ruch, and B. Michel, "Integrated microfluidic power generation and cooling for bright silicon MPSoCs," in *Proc. Conf. Design, Autom. Test Eur.*, 2014, p. 134.
[6] L. P. Giné and I. F. Akyildiz, "Molecular communication options for long range nanonetworks," *Comput. Netw.*, vol. 53, no. 16, pp. 2753–2766, 2009.
[7] A. O. Bicen and I. F. Akyildiz, "System-theoretic analysis and least-squares design of microfluidic channels for flow-induced molecular communication," *IEEE Trans. Signal Process.*, vol. 61, no. 20, pp. 5000–5013, Oct. 2013.
[8] A. O. Bicen and I. F. Akyildiz, "End-to-end propagation noise and memory analysis for molecular communication over microfluidic channels," *IEEE Trans. Commun.*, vol. 62, no. 7, pp. 2432–2443, Jul. 2014.
[9] M. Pierobon and I. F. Akyildiz, "Capacity of a diffusion-based molecular communication system with channel memory and molecular noise," *IEEE Trans. Inf. Theory*, vol. 59, no. 2, pp. 942–954, Feb. 2013.
[10] L. C. Cobo and I. F. Akyildiz, "Bacteria-based communication in nanonetworks," *Nano Commun. Netw.*, vol. 1, no. 4, pp. 244–256, 2010.
[11] M. Kuscu and O. B. Akan, "Fret-based nanoscale point-to-point and broadcast communications with multi-exciton transmission and channel routing," *IEEE Trans. Nanobiosci.*, vol. 13, no. 3, pp. 315–326, Sep. 2014.
[12] B. Krishnaswamy *et al.*, "Time-elapse communication: Bacterial communication on a microfluidic chip," *IEEE Trans. Commun.*, vol. 61, no. 12, pp. 5139–5151, Dec. 2013.
[13] J. Berthier, *Micro-Drops and Digital Microfluidics*. Oxford, U.K.: William Andrew, 2012.
[14] B. J. Kirby, *Micro- and Nanoscale Fluid Mechanics: Transport in Microfluidic Devices*. Cambridge, U.K.: Cambridge Univ. Press, 2010.
[15] P. Garstecki, M. J. Fuerstman, H. A. Stone, and G. M. Whitesides, "Formation of droplets and bubbles in a microfluidic T-junction—Scaling and mechanism of break-up," *Lab Chip*, vol. 6, no. 3, pp. 437–446, 2006.
[16] J. G. Proakis, *Digital Communications*, 5th ed. New York, NY, USA: McGraw-Hill, 2007.
[17] Y. Zhu and R. Sivakumar, "Challenges: Communication through silence in wireless sensor networks," in *Proc. 11th Annu. Int. Conf. Mobile Comput. Netw.*, 2005, pp. 140–147.
[18] Y. P. Chen, D. Wang, and J. Zhang, "Variable-base tacit communication: A new energy efficient communication scheme for sensor networks," in *Proc. 1st Int. Conf. Integr. Internet Ad Hoc Sensor Netw.*, 2006, p. 27.
[19] S. A. Wirdatmadja, "Microfluidic communications protocol design and transmission performance analysis," M.S. thesis, Dept. Electron. Commun. Eng., Tampere Univ. Technol., Tampere, Finland, 2014.
[20] E. De Leo, L. Donvito, L. Galluccio, A. Lombardo, G. Morabito, and L. M. Zanoli, "Communications and switching in microfluidic systems: Pure hydrodynamic control for networking labs-on-a-chip," *IEEE Trans. Commun.*, vol. 61, no. 11, pp. 4663–4677, Nov. 2013.
[21] J.-M. Koo, S. Im, L. Jiang, and K. E. Goodson, "Integrated microchannel cooling for three-dimensional electronic circuit architectures," *J. Heat Transf.*, vol. 127, no. 1, pp. 49–58, 2005.
[22] D. B. Tuckerman and R. F. W. Pease, "High-performance heat sinking for VLSI," *IEEE Electron Device Lett.*, vol. 2, no. 5, pp. 126–129, May 1981.
[23] W. Qu and I. Mudawar, "Experimental and numerical study of pressure drop and heat transfer in a single-phase micro-channel heat sink," *Int. J. Heat Mass Transf.*, vol. 45, no. 12, pp. 2549–2565, 2002.
[24] M. S. Bakir *et al.*, "3d heterogeneous integrated systems: Liquid cooling, power delivery, and implementation," in *Proc. IEEE Custom Integr. Circuits Conf.*, Sep. 2008, pp. 663–670.
[25] G. Türkakar and T. Okutucu-Özyurt, "Dimensional optimization of microchannel heat sinks with multiple heat sources," *Int. J. Thermal Sci.*, vol. 62, pp. 85–92, Dec. 2012.

STEFANUS ARINNO WIRDATMADJA received the bachelor's degree in electrical engineering from the Universitas Indonesia, Depok, Indonesia, in 2005. He received the master's degree in wireless communication circuits and system from the Tampere University of Technology, Finland, in 2015, where he is currently pursuing the Ph.D. degree with the Department of Electronics and Communications Engineering, Nano Communication Networks Research Group.

DMITRI MOLTCHANOV received the M.Sc. and Cand.Sc. degrees from the Saint-Petersburg State University of Telecommunications, Russia, in 2000 and 2002, respectively, and the Ph.D. degree from the Tampere University of Technology, Finland, in 2006. He is currently a Senior Research Scientist with the Department of Electronics and Communications Engineering, Tampere University of Technology. He has authored over 50 publications. His research interests include performance evaluation and optimization issues of wired and wireless IP networks, Internet traffic dynamics, quality of user experience of real-time applications, and traffic localization P2P networks. He serves as the TPC member in a number of international conferences.

SASITHARAN BALASUBRAMANIAM (SM'14) received the bachelor's degree in electrical and electronic engineering from The University of Queensland, Brisbane, Australia, in 1998, the master's degree in computer and communication engineering from the Queensland University of Technology, Brisbane, in 1999, and the Ph.D. degree from The University of Queensland in 2005. He was a Research Fellow with the Telecommunication Software and Systems Group, Waterford Institute of Technology, Waterford, Ireland, where he was involved in number of Science Foundation Ireland projects. He is currently a Senior Research Fellow with the Nano Communication Center, Department of Electronic and Communication Engineering, Tampere University of Technology, Tampere, Finland. He has authored over 70 papers and actively participates in a number of technical program committee for various conferences. His current research interests include bioinspired communication networks and molecular communications. He was the TPC Co-Chair of the ACM NANOCOM 2014 and the IEEE MoNaCom 2011 conferences, which he co-founded. He is currently an Editor of the IEEE *Internet of Things* journal and *Elsevier Nano Communication Networks*.

YEVGENI KOUCHERYAVY (SM'09) received the Ph.D. degree from the Tampere University of Technology (TUT), Finland, in 2004. He is currently a Full Professor and the Laboratory Director with the Department of Electronics and Communications Engineering, TUT. He has authored numerous publications in the field of advanced wired and wireless networking and communications. His current research interests include various aspects in heterogeneous wireless communication networks and systems, the Internet of things and its standardization, and nano communications. He is currently an Associate Technical Editor of the *IEEE Communications Magazine* and an Editor of the IEEE Communications Surveys and Tutorials.